Molecular basis for manganese sequestration by calprotectin and roles in the innate immune response to invading bacterial pathogens

Steven M. Damo[a,1], Thomas E. Kehl-Fie[b,1], Norie Sugitani[a], Marilyn E. Holt[a], Subodh Rathi[a], Wesley J. Murphy[a], Yaofang Zhang[b], Christine Betz[c], Laura Hench[a], Günter Fritz[c], Eric P. Skaar[b,2], and Walter J. Chazin[a,2]

[a]Departments of Biochemistry and Chemistry, and Center for Structural Biology, Vanderbilt University, Nashville, TN 37232-8725; [b]Department of Pathology, Microbiology, and Immunology, Vanderbilt University, Nashville, TN 37232-2363; and [c]Department of Neuropathology, University of Freiburg, 79106 Freiburg, Germany

Edited by Scott J. Hultgren, Washington University School of Medicine, St. Louis, MO, and approved January 24, 2013 (received for review November 24, 2012)

The S100A8/S100A9 heterodimer calprotectin (CP) functions in the host response to pathogens through a mechanism termed "nutritional immunity." CP binds Mn^{2+} and Zn^{2+} with high affinity and starves bacteria of these essential nutrients. Combining biophysical, structural, and microbiological analysis, we identified the molecular basis of Mn^{2+} sequestration. The asymmetry of the CP heterodimer creates a single Mn^{2+}-binding site from six histidine residues, which distinguishes CP from all other Mn^{2+}-binding proteins. Analysis of CP mutants with altered metal-binding properties revealed that, despite both Mn^{2+} and Zn^{2+} being essential metals, maximal growth inhibition of multiple bacterial pathogens requires Mn^{2+} sequestration. These data establish the importance of Mn^{2+} sequestration in defense against infection, explain the broad-spectrum antimicrobial activity of CP relative to other S100 proteins, and clarify the impact of metal depletion on the innate immune response to infection.

bacterial pathogenesis | *Staphylococcus aureus* | antibiotic resistance | protein crystal structure | isothermal titration calorimetry

Bacterial pathogens are a significant threat to global public health. This threat is compounded by the fact that these organisms are rapidly becoming resistant to all relevant antimicrobials. Of particular note is the recent emergence of antibiotic-resistant strains of *Staphylococcus aureus* as a leading cause of bacterial infection in the United States (1) and arguably the most important threat to the public health of the developed world. Consequently, the identification of therapeutics to treat bacterial pathogens is paramount to our continued ability to limit this infectious threat.

One promising area of potential therapeutic development involves targeting bacterial access to essential transition metals. This strategy is based on the fact that all bacterial pathogens require these nutrient metals to colonize their hosts (2–5). In vertebrates, the bacterial need for nutrient transition metals is counteracted by the sequestration of these metals by the host. This limitation of essential nutrients, termed "nutritional immunity," is a potent defense against infection (6). Although a variety of metals is required for microbial growth, studies of nutritional immunity have been primarily restricted to the struggle for iron (Fe) between host and pathogen (7–9).

An innate immune factor, calprotectin (CP), is abundant in neutrophils and plays a key role in nutritional immunity. CP can be found at sites of infection in excess of 1 mg/mL and is required for the control of a number of medically relevant bacteria and fungi including *S. aureus*, *Candida albicans*, and *Aspergillus fumigates* (10–14). The antimicrobial activity of CP is due to the chelation of the essential nutrients Zn^{2+} (Zn) and Mn^{2+} (Mn), which results in bacterial metal starvation and is reversed by the addition of these metals in excess (11, 13). Moreover, CP-deficient mice have increased microbial burdens following systemic challenge, underscoring the significance of Mn and Zn chelation to defense against infection (11). These findings support the possibility that metal chelation could be a general strategy to inhibit microbial outgrowth and prevent the spread of infection.

CP is a member of the S100 subfamily of EF-hand Ca^{2+}-binding proteins, which are characterized by a distinct dimeric structure. Two binding sites for Zn (and presumably other transition metals) have been identified at the dimer interface in crystal structures of Zn-bound S100B, S100A7, and S100A12 (15–17). Site-directed mutagenesis has been used to confirm that Zn and Mn are bound in the corresponding sites in CP (13). Although the inhibition of bacterial growth via metal sequestration has been established for CP, the individual contributions of Mn and Zn limitation to this process are not known (11, 13, 18). This uncertainty arises because of an inability to separate the effects attributable to the binding of Mn vs. the binding of Zn (11, 13). Knowledge of the specific Mn- and Zn-dependent processes within bacteria that are inhibited by CP is important for understanding cellular physiology and identifying new effective antimicrobial therapeutics that exploit these targets.

To address this deficiency and clarify the mechanism of CP action in nutritional immunity, we have performed a complementary series of metal-binding, structural, and microbial growth experiments on WT protein and mutants that alter Zn and Mn affinity. We prepared two complementary CP single Zn-binding-site knockout mutants and characterized their Zn/Mn binding and antimicrobial activity in bacterial growth assays. Using the variant that could not sequester Mn, we demonstrated the important contribution of Mn sequestration to nutritional immunity. A high-resolution crystal structure of Mn-bound CP revealed the critical features required for Mn binding and provided a molecular explanation for why CP is the only S100 protein that chelates Mn with high affinity. Finally, Mn sequestration was shown to be critical to the broad-spectrum antimicrobial activity of CP, underscoring the importance of CP-mediated Mn chelation by the host for the control of bacterial infection.

Results

Two Transition Metal-Binding Sites in CP Are Functionally Inequivalent. Our first goal was to determine the site responsible for Mn binding and if the two transition metal-binding sites in CP make equivalent

Author contributions: S.M.D., T.E.K.-F., E.P.S., and W.J.C. designed research; S.M.D., T.E.K.-F., N.S., M.E.H., S.R., W.J.M., Y.Z., C.B., and L.H. performed research; S.M.D., T.E.K.-F., G.F., E.P.S., and W.J.C. analyzed data; and S.M.D., T.E.K.-F., G.F., E.P.S., and W.J.C. wrote the paper.

The authors declare no conflict of interest.

This article is a PNAS Direct Submission.

Data deposition: The atomic coordinates and structure factors have been deposited in the Protein Data Bank, www.pdb.org (PDB ID code 4GGF).

[1]S.M.D. and T.E.K.-F. contributed equally to this work.

[2]To whom editorial correspondence may be addressed: walter.chazin@vanderbilt.edu or eric.skaar@vanderbilt.edu.

This article contains supporting information online at www.pnas.org/lookup/suppl/doi:10.1073/pnas.1220341110/-/DCSupplemental.

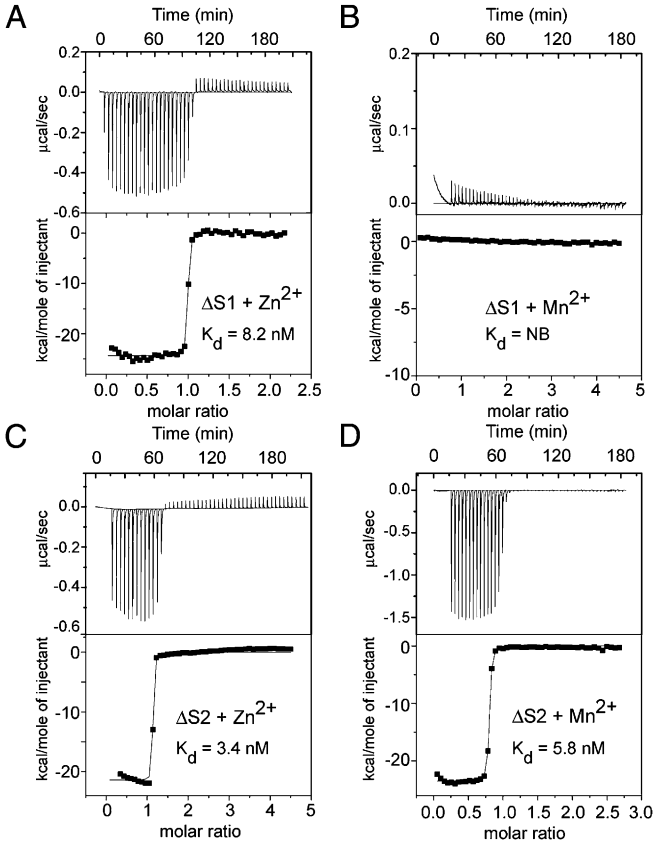

Fig. 1. Mn binds to the noncanonical transition metal-binding site in CP. (*A* and *B*) ITC titrations and binding isotherms from integrated heat for CP ΔS1 are shown for the addition of (*A*) Zn^{2+} [$K_d = 8.2 \pm 1.5$ (SD) nM] and (*B*) Mn^{2+} (no binding). (*C* and *D*) ITC titrations and binding isotherms from integrated heat for CP ΔS2 are shown for the addition of (*C*) Zn^{2+} [$K_d = 3.4 \pm 1.2$ (SD) nM] and (*D*) Mn^{2+} [$K_d = 5.8 \pm 1.6$ (SD) nM].

contributions to antimicrobial activity. To distinguish the two sites, we engineered CP mutants that contain only one active transition metal-binding site using sequence conservation and structures of Zn-bound S100 proteins as a guide (13). Canonical transition metal-binding sites in S100 proteins are formed from a conserved HXXXH motif found at the C terminus of helix 4 of one subunit in combination with a histidine and aspartate residue from the other subunit (15, 16). Whereas most S100 proteins are homodimers that have two identical transition metal-binding sites, CP is a heterodimer of S100A8 and S100A9 subunits, which results in two distinct binding sites (13, 19). Based on sequence homology and the structural similarity among S100 proteins, the first predicted site (S1) is unique among S100 proteins and is composed of residues H17 and H27 from S100A8 and of H91 and H95 from S100A9 (13, 19). The second predicted site (S2) involves residues H83 and H87 of S100A8 and of H20 and D30 of S100A9 and is similar to the canonical binding site observed in S100A7 and S100A12 (15, 16). The binding of Zn and Mn to CP was completely eradicated in a variant in which all eight of these conserved residues were mutated (13).

To selectively inactivate the noncanonical transition metal-binding site, a ΔS1 CP mutant was created with the four S1 histidine ligands changed to asparagines. To inactivate the canonical site, a ΔS2 mutant was created with the three histidines in S2 changed to asparagines and the aspartic acid to serine. Analyses of these mutants via circular dichroism spectroscopy verified that they retained their structural integrity. Isothermal titration calorimetry (ITC) was then used to measure the affinity of the mutants for Zn and Mn (Fig. 1). WT CP binds two Zn ions per heterodimer with an average dissociation constant (K_d) of 3.5 nM and one Mn ion with a K_d of 1.3 nM (13). Both ΔS1 and ΔS2 mutants bound a single Zn ion with K_d values of 8.2 ± 1.5 (SD) nM and 3.4 ± 1.2 (SD) nM, respectively. However, only the ΔS2 variant with the canonical site mutated retained high affinity for Mn [$K_d = 5.8 \pm 1.6$ (SD) nM]. These data confirm that CP possesses a single high-affinity Mn-binding site and two high-affinity Zn-binding sites and demonstrate that only the noncanonical site (S1) binds both Zn and Mn. To rule out that the antimicrobial effect of CP is due to chelation of iron, we used ITC to monitor the binding of this ion and found, consistent with previous results (11), that CP does not bind iron (Fig. S1).

Full Inhibition of *S. aureus* Growth by CP Requires Sequestration of Mn. CP inhibits bacterial growth and metal-dependent virulence factors by sequestering Mn and Zn ions. However, the relative contribution of Mn vs. Zn sequestration and the corresponding effects on specific cellular pathways are unknown (11, 13, 20). To address this issue, the ΔS1 and ΔS2 CP mutants were used to assess the individual contributions of Mn and Zn sequestration to inhibiting *S. aureus* growth. First, the 50% growth inhibitory concentration (IC_{50}) was determined for ΔS1 and ΔS2 and compared with a WT control. Values of 262 ± 120 (SD) µg/mL ($P < 0.0001$ vs. WT CP) for ΔS1 and 179 ± 68 (SD) µg/mL ($P = 0.0037$ vs. WT CP) for ΔS2 were observed, approximately twice that of WT CP [105 ± 33 (SD) µg/mL]. Control experiments to confirm that these antimicrobial effects are due to nutritional metal sequestration revealed that addition of Zn or Mn along with CP reversed the antimicrobial activity, except as expected in the case of Mn addition to ΔS1 (Fig. 2 *A*–*C*).

Remarkably, the ΔS1 mutant could not completely inhibit bacterial growth, even at concentrations in excess of 1,000 µg/mL (~40 µM). To investigate this observation further, a detailed analysis of the growth inhibitory properties of ΔS1 and ΔS2 was performed, starting with bacteria in exponential phase. The ΔS2 mutant

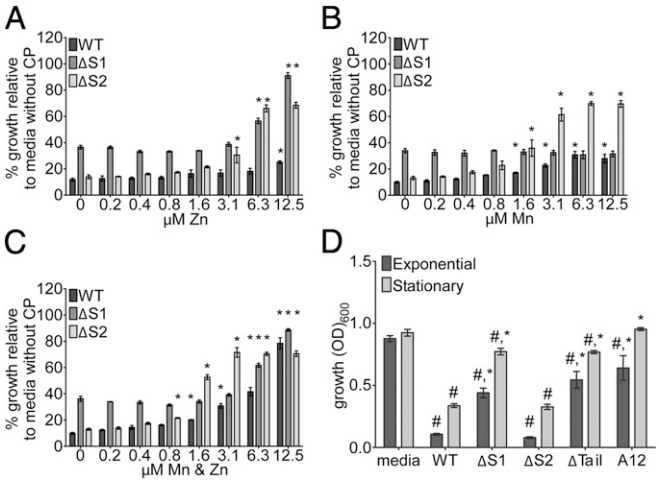

Fig. 2. Mn sequestration is necessary for inhibition of *S. aureus* growth. WT CP, ΔS1, ΔS2, ΔTail, and S100A12 were characterized for antimicrobial activity and metal binding. (*A*–*C*) *S. aureus* was incubated in the presence of 480 µg/mL WT CP, ΔS1, or ΔS2 and increasing concentrations of $MnCl_2$ and/or $ZnSO_4$. Growth was assessed by measuring OD_{600}. A single asterisk is placed above each bar for those measurements in which $P < 0.05$ (vs. media without supplemental metals) as determined from one-way ANOVA with Dunnett's posttest. (*D*) *S. aureus* was grown in media alone or with 960 µg/mL of WT CP, ΔS1, ΔS2, ΔTail, or S100A12 (A12). Cultures were started with exponential or stationary-phase bacteria, and growth was assessed by optical density (OD_{600}) at $t = 10$; $n = 3$–6. Statistical significance was determined via two-way ANOVA with Bonferroni posttest $^{\#}P < 0.05$ relative to media, and $^{*}P < 0.05$ relative to WT CP. Error bars: SEM.

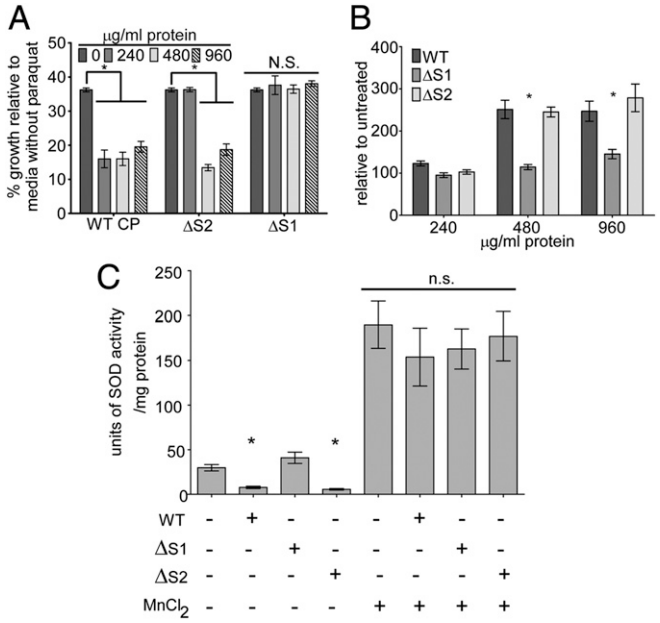

Fig. 3. Mn sequestration by CP is necessary to inhibit staphylococcal superoxide defenses. (*A*) *S. aureus* was grown in the presence of 10 mM paraquat, a superoxide-generating compound, and WT CP, ΔS1, or ΔS2. Growth was assessed by measuring optical density (OD_{600}) ($n = 4$). Significance was determined via one-way ANOVA with Dunnett's posttest. *P* values greater than 0.05 were considered not significant (N.S.). $*P < 0.001$. (*B*) The contribution of Mn binding to accumulation of oxidative stress was determined by growing *S. aureus* in the presence of WT CP, ΔS1, or ΔS2 and assessing intracellular superoxide accumulation via dihydroethidium assay ($n = 3$). Significance was determined via two-way ANOVA with Dunnett's posttest. $*P < 0.001$ vs. WT CP. *P* values greater than 0.05 were considered not significant. (*C*) To determine if inhibition of staphylococcal superoxide dismutase activity requires sequestration of Mn by calprotectin, *S. aureus* was grown in the presence of 480 μg/mL WT protein, ΔS1, or ΔS2, and SOD activity was assessed by water-soluble tetrazolium salt assay ($n = 4$). Significance was determined via one-way ANOVA with Bonferroni posttest $*P <$ 0.01 vs. WT CP. *P* values greater than 0.05 were considered not significant. Error bars represent SEM.

inhibited *S. aureus* growth throughout a time course at a level consistent with WT CP (Fig. 2*D* and Fig. S2*A*). However, even at high concentrations after an extended incubation, the ΔS1 mutant reduced *S. aureus* growth only by 50% (Fig. 2*D* and Fig. S2*A*). As both Mn and Zn are essential metals (9, 21, 22), the observation that sequestration of Zn alone by CP was insufficient to maximally inhibit *S. aureus* growth was surprising. Determination of the metal concentrations in the growth media revealed that, upon inactivation of site 1, the Zn-binding capacity of CP vastly exceeded the concentrations of Zn in either tryptic soy broth or brain heart infusion broth (Table S1). This also suggests that excess metal-binding capacity is needed to inhibit bacterial growth, most likely due to competition with bacterial high-affinity metal uptake systems (9). When similar growth experiments were performed using bacteria in stationary phase to inoculate the growth media, an even stronger dependence on Mn sequestration was observed (Fig. 2*D* and Fig. S2*B*). Overall, these results indicate that Mn sequestration by CP restricts the growth of *S. aureus* and is necessary for maximal antimicrobial activity.

Inhibition of *S. aureus* Superoxide Defenses Requires Sequestration of Manganese by CP. CP enhances the effectiveness of the neutrophil oxidative burst by inhibiting staphylococcal superoxide defenses during infection, which in turn renders *S. aureus* more sensitive to neutrophil-mediated killing (13). Specifically, CP inactivates staphylococcal superoxide dismutases (SOD) and increases the sensitivity of *S. aureus* to exogenous oxidative stress (13). Given the Mn dependency of the only two SODs expressed by *S. aureus*, SodA and SodM, it is likely that inhibition of these processes by CP is due to Mn sequestration (23, 24). To test this hypothesis, the ability of ΔS1 and ΔS2 CP to increase *S. aureus* sensitivity to superoxide, elevate intracellular superoxide levels, and reduce SOD activity was assessed. As an initial test, *S. aureus* was treated with WT CP, ΔS1, or ΔS2 and assessed for sensitivity to the superoxide-generating compound paraquat whose toxicity is greatly increased in SOD-deficient strains (13, 24, 25). WT CP and the ΔS2 mutant increased the sensitivity of *S. aureus* to paraquat whereas ΔS1 did not (Fig. 3*A*). Although in SOD-deficient strains the primary mode of paraquat toxicity is the generation of superoxide, recent work has demonstrated that this compound can exert toxic effects on bacteria independently of oxidative stress (26, 27). In light of these observations, the impact of ΔS1 and ΔS2 on intracellular superoxide and SOD activity was assessed. These studies revealed that, unlike WT and ΔS2, ΔS1 does not increase intracellular superoxide levels or inhibit *S. aureus* superoxide dismutase activity (Fig. 3 *B* and *C*). Finally, the SOD inhibitory activity of WT and ΔS2 CP was reversible upon addition of excess Mn (Fig. 3*C*). Recalling that WT and ΔS2 have the ability to bind Mn but ΔS1 does not, these results support a model whereby inhibition of staphylococcal SODs is dependent on Mn sequestration by CP.

Mode of Mn Binding by CP Is Distinct from That of Zn Binding. To determine how CP is able to bind Mn with high affinity, the structure of the Mn-bound state was determined. To eliminate complications arising from disulfide cross-linking, we used a variant of CP with S100A8 C42S and S100A9 C3S mutations, which retains wild-type antimicrobial activity [IC_{50} 100 ± 24 (SD) μg/mL vs. 105 ± 33 (SD) μg/mL] (28). The protein was crystallized in the presence of Ca^{2+} (Ca) and excess Mn, and the structure was refined to 1.6-Å resolution. The phasing of the data was determined by molecular replacement using the structure of Ca-bound CP as a search model [Protein Data Bank (PDB) code 1XK4] (19). Mn ions were identified by their anomalous signal. Four CP heterodimers were found in the asymmetric unit arranged as two pairs of dimers of heterodimers. The final model was built and refined to an R_{work}/R_{free} of 18.2%/20.5% (Table S2).

The overall secondary and tertiary structure of CP is highly homologous to previously determined structures of CP and other

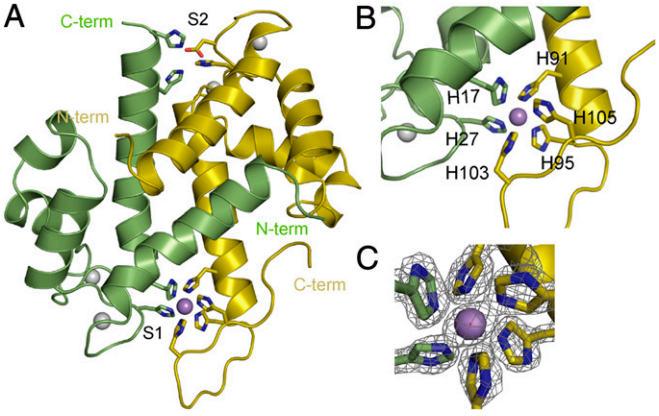

Fig. 4. X-ray crystal structure of Mn-bound CP. (*A*) Ribbon diagram of Mn-bound S100A8 (green) and S100A9 (yellow) heterodimer refined to 1.6-Å resolution. The Zn-specific (S2) and Mn/Zn (S1) binding sites are labeled. Ca ions are shown as gray spheres, and the Mn ion is shown in purple. (*B*) Close-up view of the Mn/Zn site (S1) with the six histidine residues that chelate the Mn ion labeled. (*C*) Electron density ($2F_O$-F_C map contoured at 2σ) for the Mn ion and histidine side chains showing the nearly perfect octahedral geometry.

S100 proteins (Fig. 4*A*). The S100A8 and S100A9 subunits in the heterodimer are arranged in an antiparallel fashion with the interface composed of helices 1 and 4. The dimer of heterodimers in the unit cell is stabilized by both hydrophobic and polar interactions from both subunits (19). Comparison with the Ca-CP structure shows no large conformational changes in the core four-helix bundle induced by the binding of Mn (Fig. S3*A*), consistent with the canonical transition metal-binding sites being largely preformed (29). The Cα rmsd between the Ca-bound and Ca, Mn-bound states for S100A8 residues 2–85 is 0.29 Å, and for S100A9 residues 5–90 it is 0.24 Å. The most notable difference in the structure is in the C terminus of S100A9, which is well resolved in this structure but was not observed in previous structures of the S100A9 homodimer or the CP heterodimer (Fig. S3*B*) (19, 30). In Ca, Mn-CP, this C-terminal "tail" wraps around the bound Mn ion and is highly ordered in the crystal structure. Hence, binding of the Mn ion induces a stable conformation in the otherwise flexible tail. The binding pocket created for the Mn ion is well shielded from solvent, consistent with the general tendency of metals to be bound in regions with limited exposure to solvent (31).

The crystal structure shows that the Mn ion is bound by six histidine residues: the four that are predicted to form the tetrahedral site for chelating Zn plus two additional residues from the S100A9 C-terminal tail (Fig. 4*B*). The Mn ligands in this site are H17 and H27 from S100A8 and H91, H95, H103, and H105 from S100A9. The Mn ion is coordinated in an almost perfect octahedral geometry by the Nε of the histidine side chains (Fig. 4*C*). Remarkably, no proteins in the PDB [surveyed using the Metal Interactions in Protein Structures server (32)] contain a Mn ion coordinated by six histidine side-chain ligands. The structure also reveals that, although the site involves the four conserved site 1 histidine residues, the octahedral coordination of Mn by CP is possible only because two additional histidine residues are contributed from the unique S100A9 tail.

S100A9 Tail Is Required for CP Antimicrobial Activity. To determine the contributions of the S100A9 C-terminal tail to the antimicrobial activity of CP, a S100A9 (1–102) truncation construct was used along with the WT S100A8 subunit to prepare a CP ΔTail mutant (18). Analysis of ΔTail by ITC revealed that it binds two Zn ions with high affinity but not Mn (Fig. S2 *E* and *F*). Furthermore, similar to the ΔS1 mutant, the ΔTail mutant is unable to inhibit *S. aureus* growth to the same extent as WT CP (Fig. 2*D* and Fig. S2 *C* and *D*). To isolate the effect on the Mn-chelating residues in the tail, we prepared a S100A9 triple mutant with H103, H104, and H105 replaced by asparagines (CP HN Tail). The metal-binding and antimicrobial properties of this mutant were found to closely mimic that of the ΔTail mutant (Fig. S2 *C*, *G*, and *H*). Together, these data demonstrate that high-affinity Mn binding to CP requires the S100A9 C-terminal tail and confirm that Mn binding contributes significantly to the antimicrobial activity of CP.

The importance of the unique S100A9 tail suggests that Mn binding and the ability to maximally inhibit *S. aureus* growth may be specific to CP. To evaluate this possibility, the metal-binding properties and antimicrobial activity of the neutrophil protein S100A12 were evaluated. The S100A12 homodimer has two canonical Zn-binding sites composed of H15 and D25 of one subunit and H85 and H89 of the other, making it analogous to the transition metal-binding sites found in S100A7, S100A15, and the Zn-specific site (S2) in CP (16). Consistent with the need for the distinct octahedral binding site created by the S100A9 tail, ITC analysis revealed that S100A12 is incapable of binding Mn (Fig. S2*I*). To determine if sequestration of Mn is required to maximally inhibit *S. aureus* growth and is therefore a phenomenon specific to CP, the antistaphylococcal activity of S100A12 was assessed. Similar to the ΔS1 mutant, S100A12 did not inhibit *S. aureus* growth to the same extent as WT CP when either exponential phase or stationary phase bacteria were used (Fig. 2*D* and Fig. S2 *A* and *B*). These results further establish the importance of Mn sequestration and the S100A9 tail to antimicrobial activity.

Mn Binding by CP Is Necessary for Broad-Spectrum Antimicrobial Activity. Although CP is known to inhibit the growth of a wide range of pathogens, the respective contributions of Mn and Zn sequestration to this broad antimicrobial activity have not been determined (10–13, 33). We therefore assessed the sensitivity of a panel of Gram-positive and Gram-negative bacterial pathogens including *S. aureus*, *Staphylococcus epidermidis*, *Staphylococcus lugdunensis*, *Enterococcus faecalis*, *Acinetobacter baumannii*, *Pseudomonas aeruginosa*, *Escherichia coli*, and *Shigella flexneri* to WT CP, as well as to the ΔS1 and ΔS2 mutants. CP exhibited dose-dependent growth inhibition for each of the tested pathogens (Fig. S4), consistent with a recent report for *A. baumannii* (34). Although all pathogens tested were affected, the extent of growth inhibition varied among the organisms, suggesting differences in their sensitivity to Mn and Zn limitation. Importantly, the ΔS2 mutant, which retains the ability to bind both Zn and Mn, achieved levels of growth inhibition comparable to that of WT CP (Fig. 5 and Fig. S5). In contrast, the ΔS1 mutant was unable to inhibit bacterial growth to the same extent as WT CP or the ΔS2 mutant, even at high concentrations (Fig. 5 and Fig. S5). These results confirm the broad antimicrobial activity of CP and demonstrate the essentiality of Mn sequestration for controlling the growth of medically important bacterial pathogens.

Discussion

Calprotectin has potent antimicrobial activity and is capable of inhibiting the growth of a wide range of pathogens and of reducing bacterial virulence factor activity (10–13, 33). Both of these properties are dependent on the ability of CP to bind transition metals, as the addition of excess Mn or Zn reverses these effects and a complete knockout mutant lacks antimicrobial activity (11, 13, 18). The generation of CP mutants with altered metal-binding properties provided a powerful set of reagents to assess the individual contributions of Mn and Zn sequestration to the control of microbial growth (11, 13, 18). Utilization of these mutants revealed that inhibition of staphylococcal superoxide defenses is dependent on Mn binding by CP. Furthermore, whereas Zn sequestration alone can contribute to controlling invading pathogens, maximal inhibition of a range of medically relevant pathogens was found to

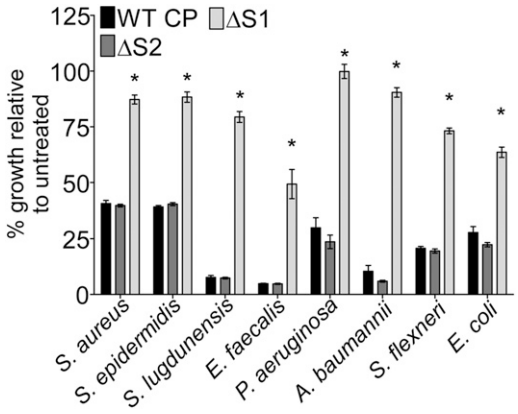

Fig. 5. Broad-spectrum antimicrobial activity of CP is dependent on Mn sequestration. *S. aureus*, *S. epidermidis*, *S. lugdunensis*, *E. faecalis*, *P. aeruginosa*, *A. baumannii*, *S. flexneri*, or *E. coli* were grown in media alone or in the presence of 960 μg/mL WT CP, ΔS1, or ΔS2. Growth was assessed by measuring optical density (OD_{600}) at 8 h. Statistical significance was determined via two-way ANOVA with Bonferroni posttest $^*P < 0.0001$ relative to WT CP; $n = 3$–4. Error bars represent SEM.

require Mn limitation. Although little is known about the role of Mn in bacterial physiology and pathogenesis, it plays critical roles in metabolism, the response to oxidative stress, and other bacterial processes (22–24). Understanding of bacterial physiology is advancing at a rapid pace, and we expect that additional Mn-dependent pathways will soon be discovered. Our results highlight the importance of Mn sequestration as a host defense mechanism to control the growth of virulent pathogens.

The C-terminal tail is unique to S100A9 among all S100 proteins, and it has been hypothesized to play a critical role in antimicrobial activity and signaling (18, 35). Previously, the ΔTail mutant was shown to have reduced antifungal activity, which was attributed to a reduced ability to bind Zn (18). The data reported here provide an alternate explanation for this result, namely that the defect in antifungal activity of the CP ΔTail mutant is due to an inability to sequester Mn.

From an evolutionary perspective, the importance of Mn sequestration to controlling infection may be reflected in the fact that there is a greater overall abundance of Mn-binding proteins in bacterial vs. eukaryotic proteomes, a consequence of the bioavailability of metal during specific time periods (36, 37). It is possible that eukaryotes evolved a defense mechanism that takes advantage of the preferential incorporation of Mn by pathogens in critical enzymes. In addition to having direct antimicrobial properties, CP is a known activator of the cell-surface receptors toll-like receptor 4 and receptor for advanced glycation end products and acts as a chemoattractant for macrophages (38, 39). Based on the observation that Mn results in structural ordering of the S100A9 C-terminal tail, it is intriguing to speculate that Mn-bound CP may have different immunomodulatory properties than Zn-bound or metal-free CP.

The Mn site in CP is unique among all structurally characterized Mn-binding proteins. The electronic structure of Mn results in a preference for oxygen vs. nitrogen coordination (40). Hence, it is surprising that the canonical S100 site with three histidines and an aspartate (S2) is not responsible for tight binding of Mn in CP. This is all the more remarkable given that a number of proteins, including superoxide dismutase from *E. coli* and MncA from *Synechocystis* PCC 6803, bind Mn tightly via three histidines and an aspartate along with a coordinating water molecule (41, 42). Mn typically binds to proteins at partially buried sites with a coordination number of five or greater where water molecules often serve as ligands in addition to side chains of the protein (41, 42). In the Mn site of CP, we propose that the lack of preferred oxygen ligands involved in Mn coordination is overcome by the creation of an almost perfect octahedral binding site that is relatively inaccessible to solvent. This line of reasoning underscores the critical importance of the S100A9 C-terminal tail in generating high affinity for Mn and, consequently, in CP's effectiveness against invading pathogens.

In addition to CP, several other S100 proteins, including S100A12, S100A7, and S100A15, have been suggested to contribute to host defense through the sequestration of essential transition metal nutrients (43–45). Numerous studies of Zn binding and crystal structures for zinc-bound S100B, S100A7, and S100A12 are available, but little is known about the Mn-binding properties of S100 proteins (15–17, 46). Analysis of the antimicrobial properties of S100A12 demonstrated that this neutrophil protein is also capable of inhibiting *S. aureus* growth. However, consistent with the inability of S100A12 to bind Mn, it is unable to achieve levels of growth inhibition similar to that of WT CP. S100A7 (psoriasin) is widely expressed on the skin and has Zn-reversible antimicrobial activity. However, the antimicrobial activity of S100A7 appears less potent than that of CP, and although it is capable of potently inhibiting *E. coli* growth, it is substantially less capable of inhibiting the growth of *S. aureus*, *S. epidermidis*, and *P. aeruginosa* (44). S100A7 has two canonical Zn-binding sites identical to the Zn-specific site in CP, and, based on our results, S100A7 would not be expected to bind Mn (15). Together, these observations support the uniqueness of CP as a potent antimicrobial factor and the important role of Mn limitation in nutritional immunity. These findings also point to variation in the importance of Zn- and Mn-dependent pathways across the spectrum of bacterial pathogens, highlighting the significance of parsing the biological roles of these two nutrient metals.

Bacterial pathogens are a significant danger to global public health, a threat that is compounded by the increasing emergence of antibiotic resistance. Understanding the molecular mechanisms of innate immunity provides insights for the development of alternative therapeutic strategies against invading organisms. CP has a key role in the host–pathogen interaction. CP endows neutrophils with a two-pronged antibacterial strategy in which it sequesters Mn and inactivates bacterial superoxide defenses at exactly the same time that bacteria are being exposed to the oxidative burst of the phagocyte. Our data define the molecular basis for CP function and elucidate the impact of Mn depletion on the innate immune response to infection. Moreover, sequestration of Mn was found to be a critical component of nutritional immunity not just against *S. aureus* but across a range of medically relevant bacterial pathogens. These results lay a foundation for development of broad-spectrum therapeutics intended to augment host-mediated nutritional immunity by exploiting Mn-dependent bacterial pathways and the unique transition metal-binding properties of CP.

Materials and Methods

Sequence Alignment, Expression, Purification, and Mutagenesis. Sequence alignments of S100A8 and S100A9 to S100A12 were performed using ClustalW (47). Generation of CP mutants and recombinant CP followed protocols as previously described (*SI Materials and Methods* and ref. 13).

Calprotectin Antimicrobial Activity Assays. Details of the strains used are provided in *SI Materials and Methods*. The IC_{50} and oxidative stress experiments were performed as previously described and are detailed in *SI Materials and Methods* (13). For growth assays, superoxide sensitivity assays, intracellular superoxide assays, and SOD activity assays, statistical analysis was performed using Graph pad Prism 5 (Graphpad Software). The statistical significance of observed differences was assessed by either two-tailed *t* test or one- or two-way ANOVA with posttest as indicated. Details of the inductively coupled plasma mass spectrometry methods used to quantify the metal levels in media are provided in *SI Materials and Methods* and Table S3.

X-Ray Crystallography. CP was diluted to 1 mg/mL (42 μM) in a buffer containing 20 mM Hepes (pH 7.5), 75 mM NaCl, and 42 μM $MnCl_2$ and then concentrated to 10 mg/mL using centrifugation through a 10-kDa membrane molecular weight cutoff. This procedure was repeated three times. Crystals were obtained by the hanging drop vapor diffusion method using 0.1 M Bis-Tris (pH 6.5), 0.2 M lithium sulfate, and 20% (mass/vol) PEG 3350. The crystals belonged to the orthorhombic space group $P2_12_12$, with unit cell dimensions of $a = 82.05$ Å, $b = 217.11$ Å, and $c = 53.12$ Å. Crystals were vitrified in liquid nitrogen using the mother liquor supplemented with 20% (vol/vol) glycerol as cryoprotectant. X-ray diffraction data were collected at a wavelength of 0.978 Å (12,677 eV) at the Advanced Photon Source at Argonne National Laboratory using the LS-CAT beamline 21-ID-F. Data were collected over 180° with a 0.6° oscillation per frame and processed with XDS (48). A second data set was collected at the Mn K edge at a wavelength of 1.88 Å (6,567 eV) at beamline 21-ID-D.

Phasing of the data was determined by molecular replacement using the program phaser with the coordinates for Ca-bound CP (PDB code 1XK4) as the search model (49). A total of four molecules were found in the asymmetric unit (Translation Function Z score 52.6). Mn ions were identified by inspection of the calculated anomalous difference maps for both data sets. Several iterative rounds of model building with Coot and refinement with Translation Libration Screw-motion using Phenix or Refmac5 were used to produce the final model (50–52). The quality and geometry of the model was evaluated with Molprobity (53, 54). The final model has a MolProbity all-atom clash score of 8.53 (76% for structures at similar resolution), and the MolProbity score is 1.85 (62% for structures of similar resolution). Coordinates and structure factors were deposited with the PDB under accession code 4GGF.

Isothermal Titration Calorimetry. CP, S100A12, and metal solutions were prepared in 20 mM Hepes (pH 7.5) and 75 mM NaCl. All solutions were

extensively degassed before titration. Titration of protein (10–50 μM) with $MnCl_2$, $Zn(OAc)_2$, or $Fe(C_6H_5O_7)$ (100–750 μM) was performed at 25 °C using a VP-ITC titration calorimeter (MicroCal Inc.). Stoichiometric $CaCl_2$ was added to the solutions before loading. A total of 50 injections of 6 μL were made for each experiment. Thermograms were corrected for heat of dilution, and binding isotherms were fit to a single-site binding model using a nonlinear least-squares curve-fitting algorithm within the software Origin 7.0. All experiments were performed in triplicate. A summary of the thermodynamic measurements is provided in Table S4.

Note Added in Proof. While this paper was under review, Nolan and coworkers reported (55) a detailed biophysical chemistry study of Mn binding to calprotectin.

1. Klevens RM, et al.; Active Bacterial Core surveillance (ABCs) MRSA Investigators (2007) Invasive methicillin-resistant *Staphylococcus aureus* infections in the United States. *JAMA* 298(15):1763–1771.
2. Andreini C, Bertini I, Cavallaro G, Holliday GL, Thornton JM (2008) Metal ions in biological catalysis: From enzyme databases to general principles. *J Biol Inorg Chem* 13(8):1205–1218.
3. Waldron KJ, Robinson NJ (2009) How do bacterial cells ensure that metalloproteins get the correct metal? *Nat Rev Microbiol* 7(1):25–35.
4. Waldron KJ, Rutherford JC, Ford D, Robinson NJ (2009) Metalloproteins and metal sensing. *Nature* 460(7257):823–830.
5. Weinberg ED (2009) Iron availability and infection. *Biochim Biophys Acta* 1790(7): 600–605.
6. Weinberg ED (1974) Iron and susceptibility to infectious disease. *Science* 184(4140): 952–956.
7. Bullen JJ (1981) The significance of iron in infection. *Rev Infect Dis* 3(6):1127–1138.
8. Hood MI, Skaar EP (2012) Nutritional immunity: Transition metals at the pathogen-host interface. *Nat Rev Microbiol* 10(8):525–537.
9. Kehl-Fie TE, Skaar EP (2010) Nutritional immunity beyond iron: A role for manganese and zinc. *Curr Opin Chem Biol* 14(2):218–224.
10. Bianchi M, Niemiec MJ, Siler U, Urban CF, Reichenbach J (2011) Restoration of anti-*Aspergillus* defense by neutrophil extracellular traps in human chronic granulomatous disease after gene therapy is calprotectin-dependent. *J Allergy Clin Immunol* 127(5):1243–1252.
11. Corbin BD, et al. (2008) Metal chelation and inhibition of bacterial growth in tissue abscesses. *Science* 319(5865):962–965.
12. Urban CF, et al. (2009) Neutrophil extracellular traps contain calprotectin, a cytosolic protein complex involved in host defense against *Candida albicans*. *PLoS Pathog* 5(10):e1000639.
13. Kehl-Fie TE, et al. (2011) Nutrient metal sequestration by calprotectin inhibits bacterial superoxide defense, enhancing neutrophil killing of *Staphylococcus aureus*. *Cell Host Microbe* 10(2):158–164.
14. Gebhardt C, Németh J, Angel P, Hess J (2006) S100A8 and S100A9 in inflammation and cancer. *Biochem Pharmacol* 72(11):1622–1631.
15. Brodersen DE, Nyborg J, Kjeldgaard M (1999) Zinc-binding site of an S100 protein revealed. Two crystal structures of Ca^{2+}-bound human psoriasin (S100A7) in the Zn^{2+}-loaded and Zn^{2+}-free states. *Biochemistry* 38(6):1695–1704.
16. Moroz OV, Blagova EV, Wilkinson AJ, Wilson KS, Bronstein IB (2009) The crystal structures of human S100A12 in apo form and in complex with zinc: New insights into S100A12 oligomerisation. *J Mol Biol* 391(3):536–551.
17. Ostendorp T, Diez J, Heizmann CW, Fritz G (2011) The crystal structures of human S100B in the zinc- and calcium-loaded state at three pH values reveal zinc ligand swapping. *Biochim Biophys Acta* 1813(5):1083–1091.
18. Sohnle PG, Hunter MJ, Hahn B, Chazin WJ (2000) Zinc-reversible antimicrobial activity of recombinant calprotectin (migration inhibitory factor-related proteins 8 and 14). *J Infect Dis* 182(4):1272–1275.
19. Korndörfer IP, Brueckner F, Skerra A (2007) The crystal structure of the human (S100A8/S100A9)2 heterotetramer, calprotectin, illustrates how conformational changes of interacting alpha-helices can determine specific association of two EF-hand proteins. *J Mol Biol* 370(5):887–898.
20. Yousefi R, et al. (2007) Human calprotectin: Effect of calcium and zinc on its secondary and tertiary structures, and role of pH in its thermal stability. *Acta Biochim Biophys Sin* (*Shanghai*) 39(10):795–802.
21. Andreini C, Banci L, Bertini I, Rosato A (2006) Zinc through the three domains of life. *J Proteome Res* 5(11):3173–3178.
22. Papp-Wallace KM, Maguire ME (2006) Manganese transport and the role of manganese in virulence. *Annu Rev Microbiol* 60:187–209.
23. Clements MO, Watson SP, Foster SJ (1999) Characterization of the major superoxide dismutase of *Staphylococcus aureus* and its role in starvation survival, stress resistance, and pathogenicity. *J Bacteriol* 181(13):3898–3903.
24. Valderas MW, Hart ME (2001) Identification and characterization of a second superoxide dismutase gene (sodM) from *Staphylococcus aureus*. *J Bacteriol* 183(11): 3399–3407.
25. Karavolos MH, Horsburgh MJ, Ingham E, Foster SJ (2003) Role and regulation of the superoxide dismutases of *Staphylococcus aureus*. *Microbiology* 149(Pt 10):2749–2758.
26. Gu M, Imlay JA (2011) The SoxRS response of *Escherichia coli* is directly activated by redox-cycling drugs rather than by superoxide. *Mol Microbiol* 79(5):1136–1150.

ACKNOWLEDGMENTS. We thank Nicole Restrepo and Dr. Seth Chitayat for assistance in the early stages of this research. This work was supported by training and operating grants from the National Institutes of Health: T32 CA009582 (to S.M.D.), T32 HL094296 (to T.E.K.-F.), R56 AI091771, R01 AI101171 (to E.P.S. and W.J.C.), R01 AI069233 (to E.P.S.), R01 AI073843 (to E.P.S.), and R01 GM62122-S1 (to W.J.C.). T.E.K.-F. was also supported by an American Heart Postdoctoral Fellowship. L.H., M.E.H., and W.J.M. were supported by the National Science Foundation–Research Experiences for Undergraduates program at Vanderbilt University. G.F. is supported by a Heisenberg fellowship of the Deutsche Forschungsgemeinschaft (FR 1488/3-1). Use of the Advanced Photon Source was supported by the US Department of Energy, Office of Science, Office of Basic Energy Sciences, under Contract DE-AC02-06CH11357. Use of the LS-CAT Sector 21 was supported by the Michigan Economic Development Corporation and the Michigan Technology Tri-Corridor (Grant 085P1000817).

27. Hassan HM, Fridovich I (1979) Paraquat and *Escherichia coli*. Mechanism of production of extracellular superoxide radical. *J Biol Chem* 254(21):10846–10852.
28. Hunter MJ, Chazin WJ (1998) High level expression and dimer characterization of the S100 EF-hand proteins, migration inhibitory factor-related proteins 8 and 14. *J Biol Chem* 273(20):12427–12435.
29. Mäler L, Potts BCM, Chazin WJ (1999) High resolution solution structure of apo calcyclin and structural variations in the S100 family of calcium-binding proteins. *J Biomol NMR* 13(3):233–247.
30. Itou H, et al. (2002) The crystal structure of human MRP14 (S100A9), a $Ca^{(2+)}$-dependent regulator protein in inflammatory process. *J Mol Biol* 316(2):265–276.
31. Dutta A, Bahar I (2010) Metal-binding sites are designed to achieve optimal mechanical and signaling properties. *Structure* 18(9):1140–1148.
32. Hemavathi K, et al. (2010) MIPS: Metal interactions in protein structures. *J Appl Cryst* 43:196–199.
33. Liu JZ, et al. (2012) Zinc sequestration by the neutrophil protein calprotectin enhances *Salmonella* growth in the inflamed gut. *Cell Host Microbe* 11(3):227–239.
34. Hood MI, et al. (2012) Identification of an *Acinetobacter baumannii* zinc acquisition system that facilitates resistance to calprotectin-mediated zinc sequestration. *PLoS Pathog* 8(12):e1003068.
35. Rammes A, et al. (1997) Myeloid-related protein (MRP) 8 and MRP14, calcium-binding proteins of the S100 family, are secreted by activated monocytes via a novel, tubulin-dependent pathway. *J Biol Chem* 272(14):9496–9502.
36. Dupont CL, Butcher A, Valas RE, Bourne PE, Caetano-Anollés G (2010) History of biological metal utilization inferred through phylogenomic analysis of protein structures. *Proc Natl Acad Sci USA* 107(23):10567–10572.
37. Dupont CL, Yang S, Palenik B, Bourne PE (2006) Modern proteomes contain putative imprints of ancient shifts in trace metal geochemistry. *Proc Natl Acad Sci USA* 103(47): 17822–17827.
38. Vogl T, et al. (2007) Mrp8 and Mrp14 are endogenous activators of Toll-like receptor 4, promoting lethal, endotoxin-induced shock. *Nat Med* 13(9):1042–1049.
39. Loser K, et al. (2010) The Toll-like receptor 4 ligands Mrp8 and Mrp14 are crucial in the development of autoreactive CD8+ T cells. *Nat Med* 16(6):713–717.
40. Harding MM, Nowicki MW, Walkinshaw MD (2010) Metals in protein structures: A review of their principal features. *Crystallogr Rev* 16(4):247–302.
41. Edwards RA, et al. (1998) Crystal structure of *Escherichia coli* manganese superoxide dismutase at 2.1-angstrom resolution. *J Biol Inorg Chem* 3(2):161–171.
42. Tottey S, et al. (2008) Protein-folding location can regulate manganese-binding versus copper- or zinc-binding. *Nature* 455(7216):1138–1142.
43. Büchau AS, et al. (2007) S100A15, an antimicrobial protein of the skin: Regulation by *E. coli* through Toll-like receptor 4. *J Invest Dermatol* 127(11):2596–2604.
44. Gläser R, et al. (2005) Antimicrobial psoriasin (S100A7) protects human skin from *Escherichia coli* infection. *Nat Immunol* 6(1):57–64.
45. Gottsch JD, Eisinger SW, Liu SH, Scott AL (1999) Calgranulin C has filariacidal and filariastatic activity. *Infect Immun* 67(12):6631–6636.
46. Charpentier TH, et al. (2008) Divalent metal ion complexes of S100B in the absence and presence of pentamidine. *J Mol Biol* 382(1):56–73.
47. Larkin MA, et al. (2007) Clustal W and Clustal X version 2.0. *Bioinformatics* 23(21): 2947–2948.
48. Kabsch W (2010) XDS. *Acta Crystallogr D Biol Crystallogr* 66(Pt 2):125–132.
49. McCoy AJ, et al. (2007) Phaser crystallographic software. *J Appl Cryst* 40(Pt 4):658–674.
50. Emsley P, Lohkamp B, Scott WG, Cowtan K (2010) Features and development of Coot. *Acta Crystallogr D Biol Crystallogr* 66(Pt 4):486–501.
51. Adams PD, et al. (2010) PHENIX: A comprehensive Python-based system for macromolecular structure solution. *Acta Crystallogr D Biol Crystallogr* 66(Pt 2):213–221.
52. Murshudov GN, Vagin AA, Dodson EJ (1997) Refinement of macromolecular structures by the maximum-likelihood method. *Acta Crystallogr D Biol Crystallogr* 53(Pt 3): 240–255.
53. Chen VB, et al. (2010) MolProbity: All-atom structure validation for macromolecular crystallography. *Acta Crystallogr D Biol Crystallogr* 66(Pt 1):12–21.
54. Davis IW, et al. (2007) MolProbity: All-atom contacts and structure validation for proteins and nucleic acids. *Nucleic Acids Res* 35(Web Server issue):W375–W383.
55. Hayden JA, et al. (2013) High-affinity manganese coordination by human calprotectin is calcium-dependent and requires the histidine-rich site formed at the dimer interface. *J Am Chem Soc* 135(2):775–787.